A generalized Born formalism for heterogeneous dielectric environments: Application to the implicit modeling of biological membranes

Seiichiro TanizakiMichael Feig

Articles you may be interested in

A generalized Born formalism for heterogeneous dielectric environments: Application to the implicit modeling of biological membranes

Seiichiro Tanizaki
Department of Biochemistry and Molecular Biology, Michigan State University, East Lansing, Michigan 48824-1319

Michael Feig[a)]
Department of Biochemistry and Molecular Biology, Michigan State University, East Lansing, Michigan 48824-1319 and Department of Chemistry, Michigan State University, East Lansing, Michigan 48824-1319

Reliable computer simulations of complex biological environments such as integral membrane proteins with explicit water and lipid molecules remain a challenging task. We propose a modification of the standard generalized Born theory of homogeneous solvent for modeling the heterogeneous dielectric environments such as lipid/water interfaces. Our model allows the representation of biological membranes in the form of multiple layered dielectric regions with dielectric constants that are different from the solute cavity. The proposed new formalism is shown to predict the electrostatic component of solvation free energy with a relative error of 0.17% compared to exact finite-difference solutions of the Poisson equation for a transmembrane helix test system. Molecular dynamics simulations of melittin and bacteriorhodopsin are carried out and performed over 10 ns and 7 ns of simulation time, respectively. The center of melittin along the membrane normal in these stable simulations is in excellent agreement with the relevant experimental data. Simulations of bacteriorhodopsin started from the experimental structure remained stable and in close agreement with experiment. We also examined the free energy profiles of water and amino acid side chain analogs upon membrane insertion. The results with our implicit membrane model agree well with the experimental transfer free energy data from cyclohexane to water as well as explicit solvent simulations of water and selected side chain analogs. © *2005 American Institute of Physics.* [DOI: 10.1063/1.1865992]

I. INTRODUCTION

Computer simulations have long been established as a powerful method for studying the structure, dynamics, and energetics of biological macromolecules.[1] In particular, the modeling of water-soluble biomolecules has become straightforward with increasingly realistic and efficient methods.[2] However, reliable simulations of more complex biological environments, such as integral membrane proteins embedded in lipid bilayers, remain a challenging task.[3] For such computer simulations, an accurate description of the surrounding environment of biological molecules is a critical aspect in achieving a realistic energetic representation of those molecules.[4] An explicit inclusion of solvent molecules provides the most detailed information on the interactions between the solute and its environment.[2,3] As an example of membrane-bound biomolecules, simulations of complex systems such as human aquaporin-1[5] and KcsA K$^+$ channels[6] with explicit lipids and water molecules have been successful in providing insightful information about their permeation mechanisms. However, due to a substantial number of solvent and lipid molecules that are needed in the

explicit representation, the majority of computer time in such simulations is typically spent on computing the detailed trajectories of the surrounding environment rather than the biomolecules of interest.[7] Furthermore, the complexity of membrane protein environments requires elaborate protocols of setting up simulation systems with explicit lipids and solvents.[8]

As an alternative to an explicit simulation, a mean field approach based on an implicit solvent description may be used to represent the environment. In such methods the solvent degrees of freedom are eliminated with a formulation that depends only on the solute conformation.[7] One successful implicit solvent approach describes the environment as a dielectric continuum, which gives rise to the solvent polarization effect described by the Poisson or Poisson–Boltzmann (PB) equations. Although numerical solutions to the PB equation accurately represent the electrostatic component of the solvent-solute interaction,[9] it remains difficult to balance efficiency and accuracy when such an approach is applied to molecular dynamics simulations of biomolecules.[10–12] However, direct application of Poisson theory has been used successfully for determining free energy profiles upon membrane insertion of rigid models of cholesterol and derived steroid hormones.[13]

[a)]Author to whom correspondence should be addressed; FAX: (517) 353-9334; Electronic mail: feig@msu.edu

A more efficient analytical approximation to solutions of the PB equation is given with the generalized Born (GB) formalism, where the electrostatic solvation free energy is expressed as an analytical pair-additive function between atoms.[14] Following recent improvements,[15–17] the GB model can predict the electrostatic solvation free energy within ~1% relative error from the exact numerical PB solution.[10] The GB model has been successfully applied to molecular dynamics simulations,[18,19] the scoring of protein confirmations in structure prediction,[20] and protein-ligand binding free energy calculations.[21]

While current GB methodology is very successful in modeling simple homogeneous dielectric environments, the implicit modeling of more complex environments, such as biological membranes, requires a heterogeneous description with a spatially varying dielectric constant. In the case of biological membranes, a layered dielectric environment with a low dielectric lipid interior surrounded by high dielectric lipid head groups and water molecules is most appropriate.[22,23] First attempts at modeling such systems with the GB model essentially treat the membrane as an extension of the solute cavity with the same dielectric constant as the solute molecule (usually $\varepsilon = 1$).[24,25] While such models were applied successful in some cases,[26] they remain fundamentally limited to a two-dielectric system (solute/membrane versus water) and do not allow a dielectric boundary between the solute and the membrane interior. The use of an empirical solvent-exclusion model in simulations of membrane proteins was also reported.[27] However, the experimental data used to derive the solvation parameters are based on the transfer free energies from vapor phase to cyclohexane, and the membrane is simply viewed as a nonpolar hydrophobic homogeneous continuum. Here, we propose a novel modification of the standard GB formalism that allows the representation of heterogeneous dielectric environments. This method (called HDGB for heterogeneous dielectric generalized Born) is illustrated with an implicit model of biological membranes, which consists of multiply layered dielectric regions. All of the layered dielectric slabs have dielectric constants that are different from the solute cavity dielectric constant.

In the following, the standard GB theory is reviewed briefly, and our modifications to the existing formalism with respect to heterogeneous environments are introduced. Then, we present and discuss results from evaluating our model for the case of a biological membrane environment with a number of test systems.

II. THEORY

A. Implicit solvent based on the generalized Born formalism

In any solvent environment, the solvation free energy of a given solute may be decomposed into electrostatic contributions ΔG_{elst}, van der Waals interactions ΔG_{vdw}, and the cost that is required for forming the solute cavity ΔG_{cavity}:[11,28,29]
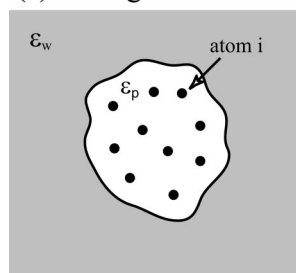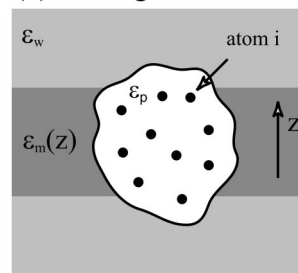

FIG. 1. (a) Homogeneous standard implicit solvent model: ε_p and ε_w are the dielectric constants of a protein and solvent, respectively. (b) Heterogeneous implicit membrane (dark gray area) environment: ε_m is the dielectric constant of a membrane and varies along the z direction.

$$\Delta G_{slv} = \Delta G_{elst} + \Delta G_{vdw} + \Delta G_{cavity}. \quad (1)$$

In a homogeneous solvent environment [Fig. 1(a); modeled as a continuous dielectric], the GB formalism expresses the electrostatic solvation free energy for a solute (represented as a set of point charges) according to the following pair-additive analytical expression:[14,30]

$$\Delta G_{elst} = -166 \left(\frac{1}{\varepsilon_p} - \frac{1}{\varepsilon_w} \right)$$
$$\times \sum_{i=1}^{n} \sum_{j=1}^{n} \frac{q_i q_j}{\sqrt{r_{ij}^2 + \alpha_i \alpha_j \exp(-r_{ij}^2/F\alpha_i\alpha_j)}}, \quad (2)$$

where ε_p is the solute cavity dielectric constant, ε_w is the solvent dielectric constant, q_i is the atomic charge of the ith atom in electron units, r_{ij} is the interatomic distance between the ith and the jth atoms in angstrom, α_i is the so-called effective Born radius of the ith atom in angstrom, and F is a dimensionless empirical parameter usually taken to be $4^{[14]}$ or $8^{[15]}$. The effective Born radius α_i is typically estimated in the Coulomb field approximation[31] (CFA) by the solute-volume integration approach, that is,

$$\frac{1}{\alpha_i} = \frac{1}{R_i} - \frac{1}{4\pi} \int_{solute,r>R_i} \frac{1}{r^4} dV \equiv A_4. \quad (3)$$

The integration is performed over the interior space of the solute except for the spherical region of a radius R_i centered at the ith atom (R_i is the van der Waals radius of the ith atom). However, it has been demonstrated that effective Born radii calculated in the Coulomb field approximation would give poor approximations to the atomic self-energies from the Poisson theory, while PB self-energies do in fact give near ideal results when Eq. (2) is used.[32] A higher order correction to the CFA was proposed in the GBMV formalism[15] as

$$\alpha_i = \frac{1}{(1 - 1/\sqrt{2})A_4 + A_7}, \quad (4)$$

where

$$A_7 = \left(\frac{1}{4R_i^4} - \frac{1}{4\pi} \int_{solute, r > R_i} \frac{1}{r^7} dV \right)^{1/4} \quad (5)$$

and A_4 is given by Eq. (3). Meanwhile other improvements to the simple CFA were proposed as well.[16,33]

Although the above formalism has become very successful in approximating the solutions to Poisson theory[34] for the high-contrast case of a low dielectric solute cavity surrounded by a high dielectric continuum (e.g., $\varepsilon_p = 1$ and $\varepsilon_w = 80$), it was recently pointed out that the effective Born radius varies according to the dielectric constant of the solvent. In fact, effective Born radii deviate increasingly from direct solutions of the Poisson equation when ε_w approaches ε_p in the low-contrast scenario of a solute in a nonpolar environment.[35] Motivated by the exact Kirkwood expression[36] for the reaction field of a single off-center charge in a solvated sphere, an expression was proposed that estimates the effective Born radius as a function of the dielectric constants of the solvent and the solute. The proposed expression is an extension of the regular GBMV formalism given in Eq. (4) and is based on the $1/r^4$ integral A_4 [Eq. (3)] and $1/r^7$ integral A_7 [Eq. (5)],

$$\alpha_i(\varepsilon_w, \varepsilon_p) = \frac{1}{C_0 A_4 + C_1 \left(\frac{3\varepsilon_w}{3\varepsilon_w + 2\varepsilon_p} \right) A_7} + D + \frac{E}{\varepsilon_w + 1}, \quad (6)$$

where C_0, C_1, D, and E are dimensionless free parameters. These four parameters are optimized with respect to the values of the electrostatic solvation energies ΔG_{elst} obtained by finite-difference solutions to the Poisson equation for a set of test proteins. The parameters were determined to be $C_0 = 0.3225$, $C_1 = 1.085$, $D = -0.14$, and $E = -0.15$, which led to a relative accuracy of ~1% with the GBMV formalism for the whole range from $\varepsilon = 80$ to low-dielectric environments.[35]

B. Extension to heterogeneous dielectric environments

In the case of a heterogeneous dielectric environment [Fig. 1(b)], it is immediately possible to introduce the idea of a local environmental dielectric constant ε_i and to calculate Born radii $\alpha_i(\varepsilon_i, \varepsilon_p)$ according to Eq. (6). While the meaning of such a local dielectric constant in the context of a heterogeneous dielectric environment will be discussed further in a moment, a modified version of Eq. (2) may then be used to obtain the solvation free energy,

$$\Delta G_{elst} = -166 \sum_{i=1}^{n} \sum_{j=1}^{n} \left(\frac{1}{\varepsilon_p} - \frac{1}{\varepsilon_{ij}(\varepsilon_i, \varepsilon_j)} \right)$$

$$\times \frac{q_i q_j}{\sqrt{r_{ij}^2 + \alpha_i(\varepsilon_i)\alpha_j(\varepsilon_j)\exp[-r_{ij}^2/F\alpha_i(\varepsilon_i)\alpha_j(\varepsilon_j)]}}, \quad (7)$$

where the prefactor $(1/\varepsilon_p - 1/\varepsilon_w)$ is now inside the double sum, and $\varepsilon_{ij}(\varepsilon_i, \varepsilon_j)$ is a function of ε_i and ε_j (see below).

Coming back to the concept of a local dielectric constant, we propose a definition based on the dielectric constant of the nearest solvent region. In the case of a biological
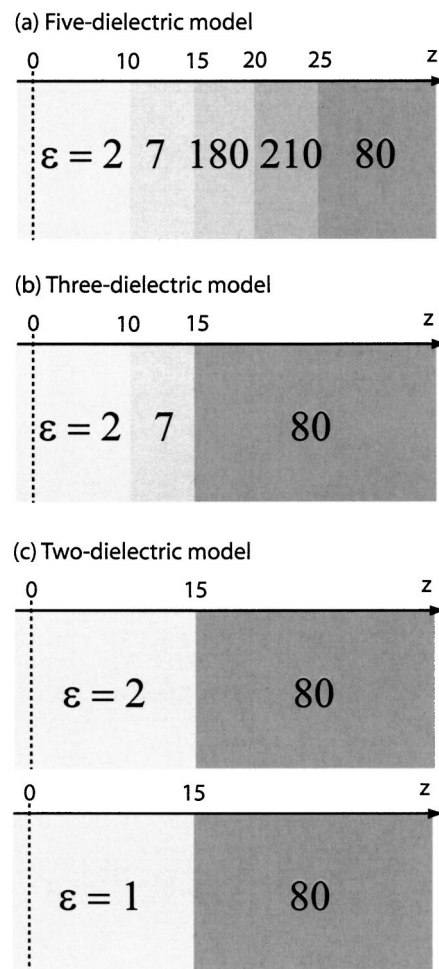

FIG. 2. Three different types of dielectric continuum models for a membrane-water system are shown schematically. The z direction corresponds to the direction normal to the membrane plane, and the center of the membrane is taken to be $z = 0$. See text for the description of the dielectric regions.

membrane the environment can be described as multiple layers of infinite dielectric continua so that the dielectric constant only varies in the direction perpendicular to the membrane (termed z in the remainder of the paper). Stern and Feller have calculated the dielectric profile of a dipalmitoylphosphatidylcholine (DPPC) lipid bilayer in water from a 20 ns molecular dynamics simulation at 50 °C and 1 atm.[22] While their analysis distinguishes between the z component and the x and y components parallel to the plane, we used their data as a guide to divide the membrane environment into different regions of isotropic dielectric media as shown in Fig. 2. We should note that throughout this study we are approximating the geometry of DPPC bilayers,[37] and we will make appropriate remarks when comparing with data for different lipid bilayers. In a five-dielectric model, the dielectric constant values are chosen to be $\varepsilon = 2$ in the membrane interior for $|z|$ between 0 and 10 Å (hydrocarbon tails of lipid molecules), $\varepsilon = 7$ for $|z|$ between 10 and 15 Å (ester group region), $\varepsilon = 180$ for $|z|$ between 15 and 20 Å (head group region), $\varepsilon = 210$ for $|z|$ between 20 and 25 Å (head group/interfacial water region), and $\varepsilon = 80$ otherwise (bulk water region). In a simpler three-dielectric model a value of 80 is
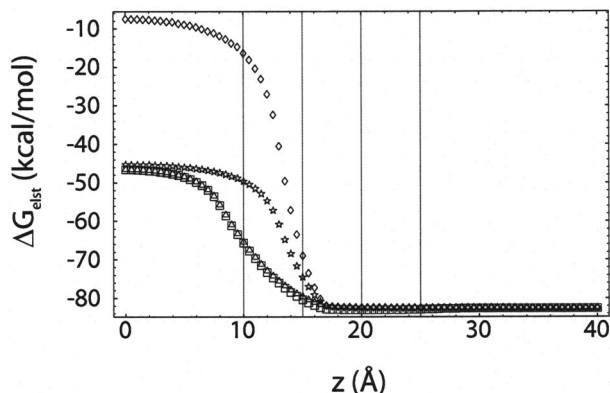
FIG. 3. The electrostatic contribution of the solvation free energy ΔG_{elst} is plotted for a monovalent spherical ion of radius 2 Å as the probe ion moves across the membrane along the z direction. Boxes and triangles represent the five- and three-dielectric models, although they may be difficult to distinguish. Stars ($\varepsilon=2$ and 80) and diamonds ($\varepsilon=1$ and 80) represent the two dielectric models. The different dielectric models for the membrane-water environment are described in Fig. 2.

assigned to the region beyond 15 Å motivated by the fact that a prefactor in Eq. (7) of $(1/1)-(1/210)$ or $(1/1)-(1/180)$ is approximately equal to $(1/1)-(1/80)$. A two-dielectric model was also considered in which the membrane is a homogeneous dielectric medium with $\varepsilon=1$ (model B) or $\varepsilon=2$ (model A) from 0 to 15 Å from the center. In all of these cases, the most straightforward approach would be to simply use the stepwise function $\varepsilon(z)$, which maps the dielectric constants of the underlying layers and to define the local dielectric constant for an atomic site according to its position. This is problematic, however, because it neglects the effect of polarization at the dielectric boundaries that are present in a layered dielectric system in addition to any issues that arise due to discontinuities at the layer interfaces. In fact, if one considers the case of a spherical ion in the context of one or more planar dielectric interfaces, the electrostatic solvation energy obtained by solving the Poisson equation varies smoothly as a function of the z coordinate normal to the interfaces (see Fig. 3).

If the solvation energy was only dependent on the dielectric environment of the layer where the center of the ion is located, the solvation energy could be calculated according to the Born equation[38] and would be constant within each dielectric layer, which is clearly not the case in this example. While Poisson theory treats the case of multiple dielectric boundaries correctly by solving the electrostatic potential throughout space, the GB formalism is inherently local and cannot explicitly incorporate additional dielectric interfaces that may be present in a given system. As a solution to this problem, we propose the introduction of an apparent dielectric constant at a given spatial location in the heterogeneous continuum environment, which reflects the effect of the entire environment on a probe at that location. This apparent local dielectric constant, termed $\varepsilon'(z)$, is obtained by solving the Born equation[38] in the case of a suitable spherical probe with the electrostatic solvation energy $\Delta G_{elst}(z)$ obtained from Poisson theory,
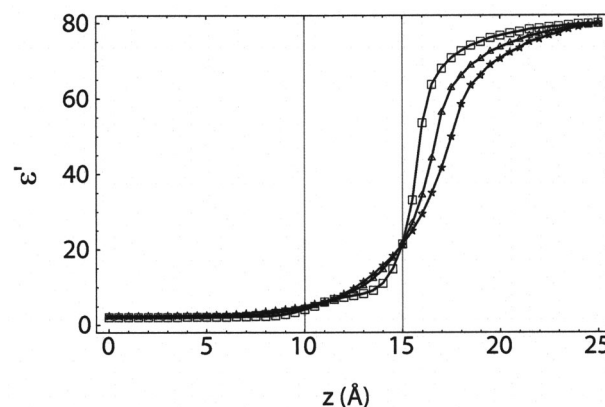

FIG. 4. The apparent dielectric constant curves are determined for the probe ions of three different radii (box for 1 Å, triangle for 2 Å, and star for 3 Å). The values of ε' at the center of the membrane for radii 1, 2, and 3 Å are 2.108, 2.258, and 2.426, respectively.

$$\Delta G_{elst}(z) = -166\left(1 - \frac{1}{\varepsilon'(z)}\right)\frac{q^2}{a}, \qquad (8)$$

where q is a charge value of the probe ion (1 for the monovalent ion) in electron units and a is a radius of the ion sphere in angstrom.

In the case of our membrane model, the calculation of such an apparent dielectric constant is simplified by the membrane geometry and only depends on the z direction. Figure 3 shows the electrostatic solvation free energy $\Delta G_{elst}(z)$ of a monovalent spherical ion computed numerically by solving the Poisson equation as the ion moves across the implicit membrane models described in Fig. 2. The radius of the ion was set to be 2 Å. In comparing the different models proposed above, we find that the maximum absolute difference in ΔG_{elst} between the five-dielectric model and the three-dielectric model is less than 0.9 kcal/mol while the difference between the five-dielectric model and two-dielectric model A is substantial (up to 19 kcal/mol). We also note that in the two-dielectric model B the transfer free energy of an ion from bulk water to the membrane center is almost twice as large compared to all other models. From this comparison, it appears that the three-dielectric model is sufficient in capturing the essential dielectric properties of biological membranes while the two-dielectric model introduces rather large deviations from the most comprehensive five-dielectric model. Figure 4 shows the resulting apparent dielectric constant curves determined from Eq. (8) by using three different probe radii (1, 2, and 3 Å) for the three-dielectric model with dielectric constants of 2, 7, and 80. We would like to emphasize that the calculated apparent dielectric constant profile depends on the specific dielectric environment, and the profile will have to be recalculated for a different system, for example, for a membrane with a different width. While this is somewhat inconvenient, such a calculation only needs to be performed once for a given system. Since a suitable analytical description of the curves in Fig. 4 is not readily available, we decided to employ a cubic spline interpolation function with first derivatives set to zero at end points (0 and 25 Å), which results in a differentiable function needed for molecular dynamics

simulations.[39] Based on such a function we then set $\varepsilon_i = \varepsilon'(z_i)$ and determine the effective Born radius α_i of the ith atom from Eq. (6) for the apparent local dielectric constant $\varepsilon'(z_i)$. In order to calculate ε_{ij} in Eq. (7), we propose the simple arithmetic mean:

$$\varepsilon_{ij} = \tfrac{1}{2}[\varepsilon'(z_i) + \varepsilon'(z_j)]. \tag{9}$$

C. Nonpolar contributions to the solvation free energy

The nonpolar contribution to the solvation free energy is especially important in heterogeneous environments. While many biomolecules remain stable in aqueous solvent just based on internal interactions and the electrostatic contribution to the solvation free energy, a varying nonpolar solvation free energy is essential in allowing molecules to remain in low-dielectric regions of heterogeneous environments. Based on the electrostatic interactions alone, any molecule would always be driven to the region of highest dielectric constant, where the screening of charge-charge interactions is maximized. Nonpolar contributions counteract the electrostatic effect, as they are usually more favorable in low-dielectric environments such as the interior of biological membranes. In the case of hydrophobic residues with a small electrostatic component, the nonpolar contribution wins out so that such entities become favorable in low-dielectric regions.

The nonpolar contribution to the solvation free energy is often approximated by a function that depends linearly on the solvent-accessible surface area,[14,40,41] summarizing both the cost of cavity formation and van der Waals solute-solvent interactions. While the solvent-accessible surface area model approximates the cost of cavity formation quite well,[40] we note that recent efforts are under way to modify this formalism in order to obtain a more accurate account of van der Waals solute-solvent interactions.[16,28] For the purposes of this study, we continue to use the standard solvent-accessible surface area model for the entire nonpolar contribution, while possible improvements with regard to van der Waals terms in the context of a heterogeneous environment are deferred to a later study. In biological membrane environments,
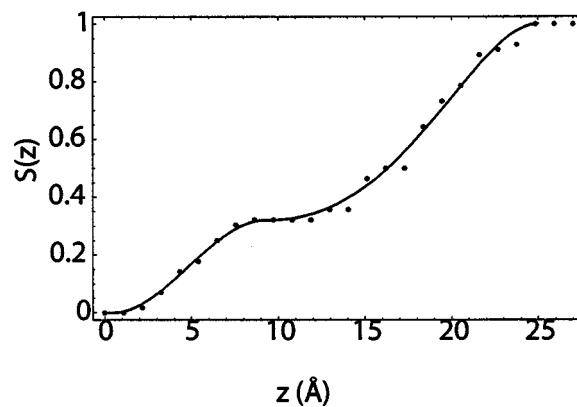

FIG. 5. The profile function $S(z)$ (solid line) was derived by least-squares fit to the free energy profile data of oxygen in the lipid membrane computed by explicit MD simulations show as points (data are normalized to one) (Ref. 43).

the nonpolar contribution is assumed to vary only along the z direction. Therefore, we will use the following functional form:

$$\Delta G_{np} = \Delta G_{vdw} + \Delta G_{cavity} = \gamma \sum_{i=1}^{n} S(z_i)SA_i, \tag{10}$$

where SA_i is a solvent-accessible surface area of the ith atom, γ is an empirical surface tension parameter to be determined, and $S(z)$ introduces the variation of the surface tension along the z direction.

In previous studies, a simple and relatively steep switching function was used to describe the change in the surface tension parameter from lipid membrane to bulk water.[24,42] Such a switching function is basically motivated by a step function of low surface tension inside the membrane and high surface tension outside, which may fit well with a simple two-dielectric model, but is insufficient in combination with the more detailed, layered membrane model proposed here. A detailed free energy profile of O_2 upon insertion in the lipid membrane has been computed by the explicit molecular dynamics (MD) simulation.[43] Assuming that the solvent-accessible surface area is constant regardless to the position of oxygen, we used this data to define the shape of $S(z)$ in Eq. (12) as shown in Fig. 5. In order to fit the data from explicit MD simulations[43] the following analytical and differentiable function was used:

$$S(z) = \begin{cases} c(|z| - z_a)^2(3z_b - 2|z| - z_a)/(z_b - z_a)^3 & (0 \leq |z| < z_b) \\ (1-c)(|z|^2 - z_b^2)^2(3z_c^2 - 2|z|^2 - z_b^2)/(z_c^2 - z_b^2)^3 & (z_b \leq |z| < z_c) \\ 1 & (\text{otherwise}). \end{cases} \tag{11}$$

The values of parameters c, z_a, z_b, and z_c were determined to be 0.32, 0.5, 9.2, and 25 Å, respectively. As the nonpolar contribution is essentially zero in the membrane interior[43] and the function $S(z)$ is scaled to the interval [0, 1], the value of γ in Eq. (10) should reflect the surface tension in aqueous

solvent. Other studies have used water surface tension parameters from 5[40] to 33[8], with lower values justified by experimental transfer energies for the alkane series[40,44] and successful folding studies of peptides with implicit solvent.[45] We tested different values in this range and found that values

between 5 and 15 cal/mol/Å^2 give best results. In the following we will show results for 5, 10, and 15 cal/mol/Å^2 in order to demonstrate the effect of this parameter.

III. METHODS

The new formalism for modeling biological membranes with the heterogeneous dielectric GB method in the preceding section was implemented based on the GBMV method[15] in the macromolecular simulation package CHARMM,[46,47] version c30b0. All charge values and van der Waals radii used are taken from the standard CHARMM22 force fields and parameters.[47] All hydrogen atoms are constructed by using the HBUILD module in CHARMM program. Exceptions are noted otherwise.

A. Test systems

In order to test the agreement between our new HDGB model and Poisson theory we generated 64 different orientations of the M2 channel-lining segment from nicotinic acetylcholine receptors and computed the electrostatic solvation free energies for each orientation. The experimental structure of M2 [PDB entry 1EQ84 (Ref. 8)] was manually rotated at nine different angles and translated in seven different increments from the center of the membrane in order to span interior and exterior regions of the lipid bilayer. For this comparison, we used the three-dielectric model of the membrane-water system for our membrane GB calculation (Fig. 6). The reference values for the electrostatic solvation free energy were computed by solving the Poisson equation with the finite difference method implemented in the PBEQ module[42,49] of CHARMM program. The focusing method was used. The grid spacing was reduced from 0.8 Å to 0.2 Å via 0.4 Å. A water probe radius of 1.4 Å was used to define the molecular surface. We assessed the reliability of our membrane GB theory including the nonpolar contributions by analyzing several test systems. Different values of the surface tension parameters (5, 10, and 15 cal/mol Å^2) were used to estimate the effect of their magnitude for all simulations with exceptions noted. Solvation free energy profiles in the lipid membrane were calculated for an SPC water molecule[50] and amino acid side chain analogs. For the case of amino acid side chain analogues, our implicit membrane GB model as well as the two-dielectric model GBSW (Refs. 24 and 26) was used for comparison. For GBSW calculations, we used 0.04 kcal/mol Å^2 with a membrane thickness of 30 Å.

Molecular dynamics simulations of melittin from bee venom and bacteriorhodopsin (bR) from *Halobacterium salinarum* were performed with our HDGB model. The details of force field parameters of the protonated retinal Schiff base can be found in Saam *et al.*[51] For both molecular dynamics simulations we employed the recently improved CMAP ϕ/ψ torsion potential.[18] The starting structures of melittin and bacteriorhodopsin were taken from the x-ray crystallographic structures [PDB entry 2MLT (Ref. 52) and 1QHJ,[53] respectively]. Melittin was terminated with a charged C terminus and a neutral N terminus.[8] Its center of mass was placed at

$z=19$ Å initially. Bacteriorhodopsin was terminated with a charged standard terminus at both ends, and its center of mass was placed at membrane center ($z=0$). Standard protonation states were used for all amino acids of bacteriorhodopsin except that the residues Asp96 and Asp212 were protonated.[27,54] The systems were heated from 0 K to 300 K for 135 ps for melittin and 160 ps for bacteriorhodopsin while the harmonic constraint on the backbone atoms of melittin was released gradually. The temperature of the system was controlled by using Langevin dynamics with a friction coefficient of 5 ps^{-1} for all atoms except for hydrogen. The SHAKE algorithm[55] was used to fix the bond length to hydrogen atoms, which allowed a simulation time step of 2 fs.

IV. RESULTS

A. Membrane generalized Born model versus Poisson theory

The electrostatic solvation free energies from the HDGB formalism were computed by using the three apparent dielectric constant profiles for probe radii of 1, 2, and 3 Å (see Fig. 4). The comparison with the PB reference values is shown in Fig. 7. We found that the relative errors S between our HDGB model and the PB reference values are 0.39% for the 1 Å radius, 0.17% for the 2 Å probe radius, and 0.50% for the 3 Å probe radius. While all of these values show excellent agreement between HDGB and PB theory, the agreement is best when the apparent dielectric profile for the 2 Å probe radius is used. Based on these results, we used the apparent dielectric profile of the 2 Å probe radius in all other calculations. The choice of a 2 Å probe also agrees best with the typical distance of heavy atoms from the molecular surface.

B. Free energy profile of water and amino acid side chain across membrane

As a first test of our membrane model, we studied the free energy profile of water and amino acid side chain ana-
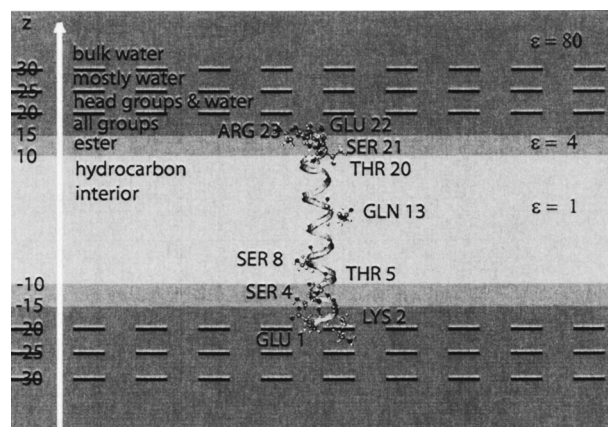

FIG. 6. The M2 channel-lining segment from nicotinic acetylcholine receptors [PDB entry 1EQ8 (Ref. 48)] is placed in the membrane-water system which is modeled as three dielectric media (hydrocarbon interior, ester group, and the rest). The partition of the membrane-water system into different regions is based on explicit simulations (Ref. 22).
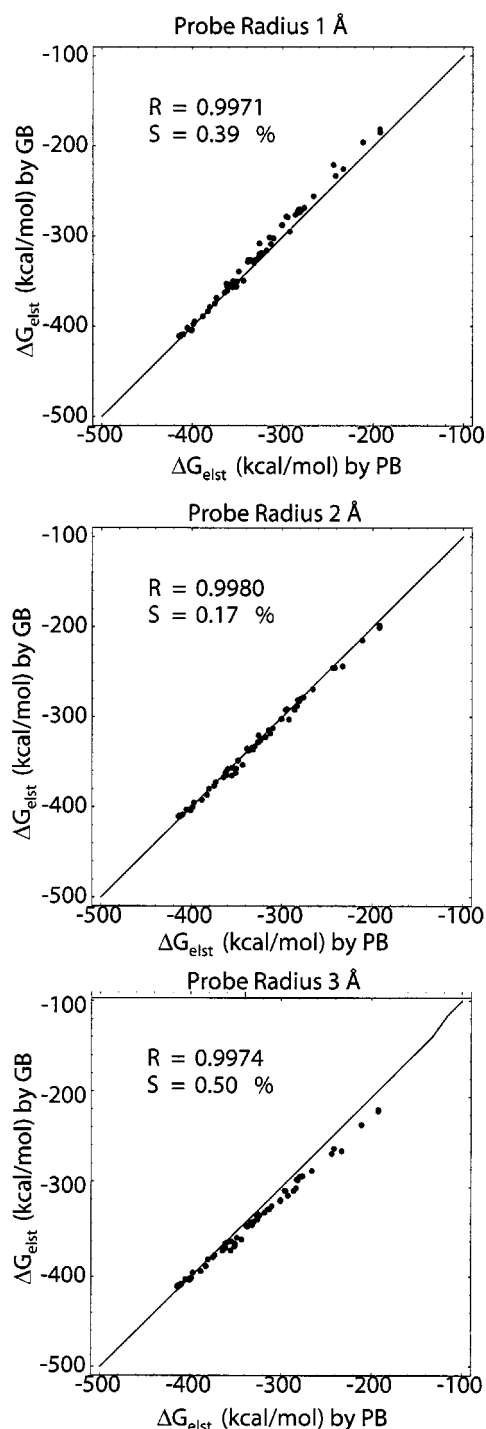
FIG. 7. Electrostatic solvation free energies are calculated for 64 different orientations and positions of M2 by using three different apparent dielectric constant profiles (see Fig. 4), and compared with the CHARMM PBEQ results.
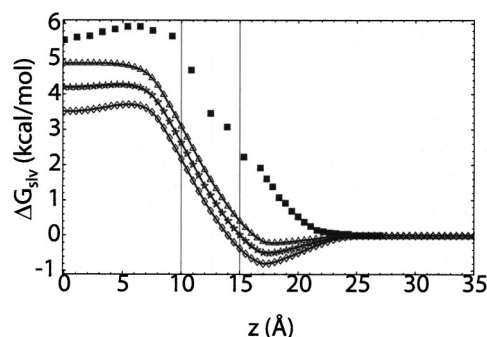

FIG. 8. Solvation free energy profile of water molecule along the z axis with different values of surface tension parameters (triangles for 5 cal/mol Å^2, stars for 10 cal/mol Å^2, and diamonds for 15 cal/mol Å^2). Explicit MD simulation data are shown as filled boxes (Ref. 56).

logs upon membrane insertion based on the three-dielectric implicit membrane model. In these tests we added the nonpolar contribution based on the solvent-accessible surface area model as described in Sec. II. For the SPC water model, a free energy profile is available from explicit MD simulations of water and DPPC lipid molecules.[43,56] In order to match the explicit model as closely as possible, some modifications of our model were necessary. SPC water underestimates the dielectric constant of bulk water with a value of 65.[57] We scaled the apparent dielectric constant profile to

yield a matching value of 65 in the bulk water region rather than 80. We also modified the oxygen radius of the SPC model, which is used to define the dielectric boundary, to a value of 1.8950 Å so that the electrostatic solvation energy of −8.4 kcal/mol found from explicit MD simulation for the SPC model[58] is reproduced by the implicit model. Assuming a fixed conformation, the free energy profile of water and amino acid side chain analogs upon membrane insertion were obtained from averaging the solvation free energy for different orientations at a given fixed center-of-mass distance z from the membrane center.

In Fig. 8, the free energy profiles for the SPC water model, computed with three different surface tension parameters (5, 10, and 15 cal/mol Å^2), are compared with the profile from the explicit MD simulation. While the overall agreement is good for the implicit nature of our model, we find deviations in the transfer free energy from water to the membrane center of about −0.5, −1.0, and −1.5 kcal/mol for surface tension parameters of 5, 10, and 15 cal/mol Å^2, respectively. A shallow minimum in the implicit free energy profile on the order of kT is located in the region around 17 Å which is not present in the data from the explicit MD simulation and becomes more pronounced with increasing surface tension values.

One possible explanation of the discrepancy between our model and the explicit MD simulation results is that it has been assumed so far that the solvent-accessible molecular surface remains constant along the z direction inside and outside of the membrane. The effect of the change in the effective excluded molecular volume from bulk water to membrane is probably not negligible. For a small spherical molecule such as water, lipid molecules are unlikely to be able to wrap around the small high-curvature spherical surface, whereas near perfect packing is possible in aqueous phase. As a result, the effectively excluded volume of water inside the lipid membrane could be increased substantially. While we plan to investigate this question in detail with explicit lipid MD simulations that are beyond the scope of the present study, we can roughly estimate the effect of the volume change based on the difference in the free energy profiles between our membrane GB model and explicit MD simulations. The electrostatic contribution to the solvation free energy is modulated strongly by a change in the
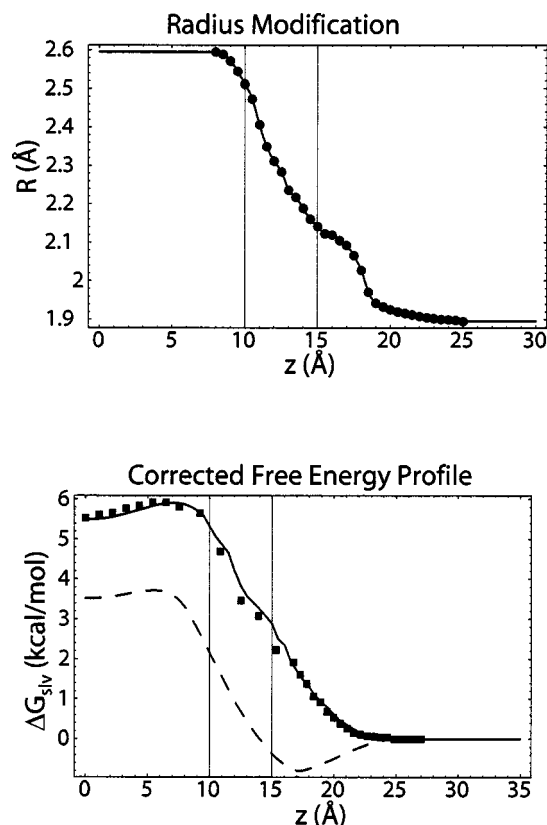
FIG. 9. Change in water oxygen radius (top) for $\gamma = 15$ kcal/mol Å^2 in order to match the free energy profile (bottom) between our implicit membrane model (solid line) and data from explicit MD simulations (filled box). The uncorrected solvation free energy profile (dotted line) is shown for comparison.
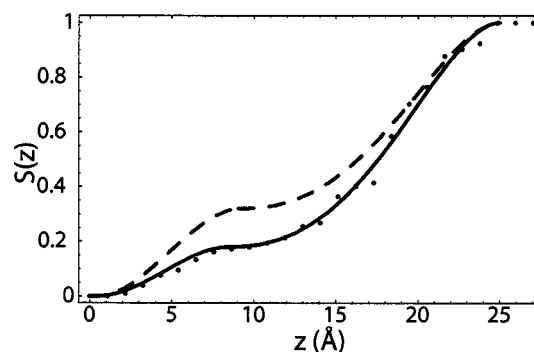

FIG. 10. Nonpolar profile $S(z)$ (solid line) corrected according to the suggested change in the water oxygen radius inside the membrane as shown in Fig. 9. The original profile from Fig. 5 (dotted line) is shown for comparison.

excluded volume as given by the choice of atomic radii that define the excluded volume in the implicit model. In the case of water, only the oxygen radius is relevant, since the hydrogen atoms are embedded completely within the van der Waals sphere of the water oxygen. Therefore, the free energy profile of water can be matched by altering the oxygen radius suitably as a function of z. As a result we obtained the oxygen radius profile (shown in Fig. 9 top), which leads (by construction) to very close agreement of the free energy profiles from implicit solvent and the explicit simulations (Fig. 9 bottom). Here, we did not change the nonpolar contribution based on oxygen (Fig. 5), since the nonpolar profile of water was found to be very similar to the oxygen from explicit lipid simulations.[43,56]

However, in the case of larger molecules, the standard set of atomic radii is assumed to be appropriate for the electrostatic contribution to the solvation free energy because a much closer contact is possible between the lipids and a low-curvature molecular surface. However, the nonpolar contribution, which is based on the small oxygen molecule, may need to be corrected for large molecules for the same reason the electrostatic contribution is corrected for water. If we assume that the correction of the water oxygen radius as a function of z (Fig. 9 top) is indicative of how the effective excluded volume is enlarged in the membrane interior, we can use that data to estimate the correction of the nonpolar contribution for large molecules. As a result we obtained the

profile shown in Fig. 10 with the parameters c, z_a, z_b, and z_c in Eq. (11) determined to be 0.18, 0.5, 8.5, and 25 Å, respectively. We tested the modified nonpolar curve with a new MD simulation of melittin with the results described below.

In Fig. 11, the free energy profile of neutral amino acid side chain analogs across three-dielectric model membrane were computed without any radius modification (uncorrected) and with the radii of all atoms scaled according to the ratio given in Fig. 9 (corrected). We also computed the free energy profiles by using the two-dielectric implicit membrane model GBSW (Refs. 24 and 26) for comparison. For methanol, acetamide, and acetic acid, explicit MD simulation results[59] were available and are shown as well. For these free energy profile calculations, we used a surface tension parameter of 15 kcal/mol Å^2 since we found that this choice best described the position of melittin in membrane from the molecular dynamics simulations of melittin (described below). Table I summarizes our results showing the free energies of transfer from the center of the membrane to bulk solvent for uncharged species at pH$=7$. Amino acid side chain analogs are arranged in increasing order of the solvent accessible surface area (SASA). For molecules with SASA less than 270 Å^2 except 4-methylimidazole, the agreement of our model with the experimental free energies of transfer from cyclohexane to water is better with the radius modification applied. For toluene, p-cresol, and 3-methylindole, SASA is close to or bigger than 300 Å^2, and the agreement is better without the radius modification. This result is consistent with the idea that larger molecules can be packed more efficiently in the lipid environment. The free energy of transfer for 4-methylimidazole is computed more accurately without the radius correction although it has SASA less than 270 Å^2. The shape of 4-methylimidazole is, however, planar, and a closer contact is possible between the lipids if the small molecule is oriented vertically. The errors of our model are within about 1.5 kcal/mol when the radii are modified for the smallest molecules as suggested. These results may be compared with aqueous solvation free energies from extremely accurate explicit solvent simulations that have resulted in an error of 1.06 kcal/mol for the CHARMM force field for 15 neutral amino acid side chain analogs.[60] In comparing with the explicit membrane insertion profiles from a recent study,[59] we find that the implicit free energy profiles with our new for-
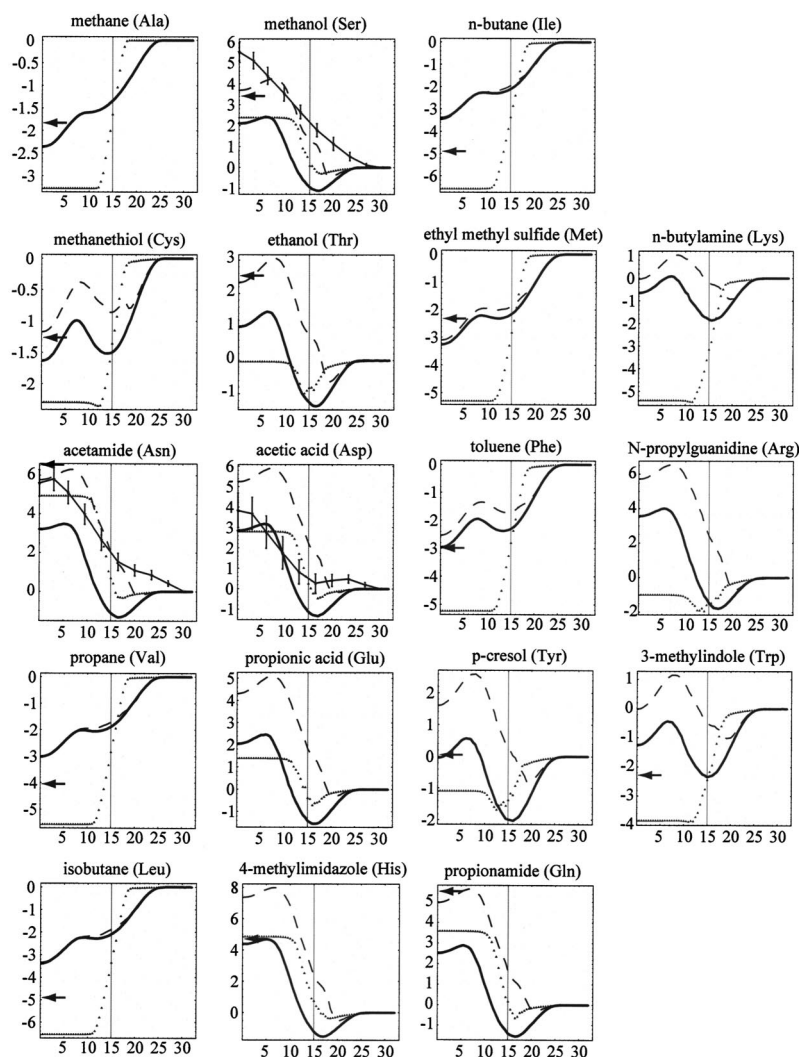
FIG. 11. Solvation free energy profiles of amino acid side chain analogs along the z axis are shown for our implicit model GB model without the radius correction (solid line) and with the radius correction (dashed line), the two-dielectric model GBSW (Ref. 24) (empty triangle), and the explicit MD simulation results (Ref. 59) (solid line with error bar; only for methanol, acetamide, and acetic acids). We used surface tension parameters of 15 cal/mol Å^2. The arrow indicates the experimental transfer free energy from cyclohexane to water for uncharged species (Ref. 74) at pH 7.

malism agrees well with the data available for Asn, Asp, and Ser analogs. The results of the two-dielectric model GBSW do not agree with the experimental results as well as our model, especially for Met and Phe analogs the errors were larger than 2 kcal/mol. Furthermore, there are qualitative differences with the GBSW model for ethanol (which should be less favorable in the membrane interior) and for all of the aromatic molecules as described below.

Aromatic residues (Tyr, Trp, and Phe) are known to be located predominantly in the membrane interface regions of membrane proteins.[61,62] This observation has been quantified further by neutron diffraction measurements of the transbilayer distribution of Ala-Trp-Ala-*O-tert*-butyl peptide in oriented dioleoyl phosphatidylcholine (DOPC) bilayers. The distribution of its geometrical center was described by the combination of two Gaussian functions and resulted in the rather broad range from 9.5 Å to 33.1 Å with the center located at 24.30 Å from the bilayer center.[63] Our HDGB model, without any radius modification, predicted the location of free energy minimum of Tyr and Trp analogs at 16.0 Å and 15.0 Å, respectively (Fig. 11), which were just above the ester group region for all values of the surface tension parameter. For Phe analog, the free energy minimum was not observed around interface. The predicted value for

Trp analog is at the lower end of the experimental range for the location of the Trp residue of Ala-Trp-Ala-*O-tert*-butyl peptide, but close to the average location of tryptophan residues in a number of membrane proteins[61] and the results of explicit MD simulations of indole molecule.[64] The transfer free energy of 3-methylindole from water to membrane was estimated by our model to be −2.3 kcal/mol, which qualitatively agrees with the range of experimental values.[27,63,65] The two-dielectric membrane model GBSW did not predict a free energy minimum at the interface for any of the three aromatic compounds which is expected to have an effect in simulations with GBSW where the localization of aromatic residues at the interface plays an important role. The empirical solvent-exclusion model of membrane proteins by Lazaridis estimated the transfer free energy of 3-methylindole from water to the interface to be −1.7 kcal/mol, which is in agreement with our results. The position of the Trp residue of Ala-Trp-Ala-*O-tert*-butyl peptide was found to be 14.5 Å in his two-dielectric representation of biological membranes, which is also similar to our results for 3-methylindole. However, more experimental and simulation data may be needed in order to assess the accuracy of our implicit model in more detail.

TABLE I. Free energies of transfer from the center of the membrane to bulk solvent for neutral amino acid side chain analogs are computed without the radius modification (uncorrected) and with the radius modification (corrected). They are arranged in increasing order of the solvent accessible surface area (SASA) and compared with the experimental data (Ref. 74) and results from the two-dielectric model GBSW (Refs. 24 and 26). Boldface is used in uncorrected and corrected columns to indicate the value that agrees better to experimental data.

Solute	SASA (Å^2)	Expt. (kcal/mol)	Uncorrected (kcal/mol)	Corrected (kcal/mol)	GBSW (kcal/mol)
Methane	157.0	1.81	2.36	2.36	3.28
Methanol	181.1	−3.40	−2.11	**−3.69**	−2.38
Methanethiol	193.8	1.28	1.63	**1.17**	2.29
Ethanol	210.5	−2.57	−1.00	**−2.33**	0.03
Acetamide	219.7	−6.64	−3.21	**−5.77**	−4.94
Propane	231.5	4.04	3.02	**3.03**	5.57
Propionamide	252.0	−5.54	−2.52	**−4.98**	−3.59
Isobutane	256.3	4.92	3.36	**3.41**	6.54
n-butane	260.0	4.92	3.40	**3.46**	6.57
4-methylimidazol	260.6	−4.66	**−4.38**	−7.37	−4.86
Ethyl methyl sulfide	266.8	2.35	3.26	**3.10**	5.29
Toluene	298.1	2.98	**2.96**	2.53	5.23
p-cresol	312.5	−0.14	**0.04**	−1.01	1.09
3-methylindole	341.2	2.33	**1.25**	0.01	3.84

C. Molecular dynamics simulations of melittin from bee venom

Melittin is an amphipathic membrane-lytic α-helical peptide with 26 amino acid residues found in bee venom.[52] Melittin has become a benchmark system for membrane environments with an extensive accumulation of experimental and computational data. The location of melittin (defined as the projection of the atomic coordinates along the bilayer normal) in oriented DOPC bilayers was determined at 17.5 Å from the membrane center with a Gaussian width of 4.3 Å by x-ray crystallography using an absolute-scale refinement method.[66]

Figure 12 shows the trajectory of the z component of geometrical center of melittin over 10 ns of MD simulation with different surface tension parameters. The switching function in Fig. 5 was used. Since our membrane model describes the DPPC lipid membrane, we adjusted the positions from experiments and the explicit MD simulations in
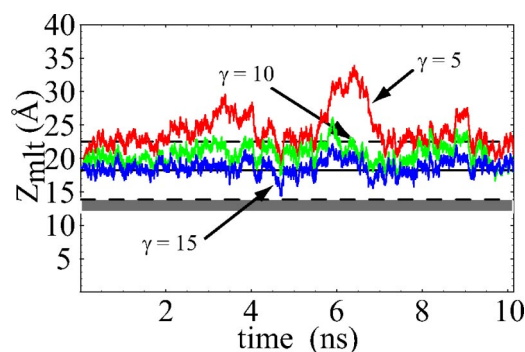

FIG. 12. Z component of the geometrical center of melittin over 10 ns of MD simulation at 300 K for different surface tension parameters. Horizontal dotted lines indicate the experimental distribution. The shaded area corresponds to the range of the center of mass position of melittin during a 600 ps molecular dynamics simulation of melittin in explicit lipid bilayers and water (Ref. 8).

Fig. 12 based on the difference in the thickness of the hydrocarbon core between DPPC and DOPC (28.5 Å for DPPC and 27.1 Å for DOPC).[37] The geometric center of melittin averaged over the last 2 ns of our simulations were found to be 22.9, 20.5, and 19.1 Å for surface tension values of 5, 10, and 15 cal/mol Å^2, respectively (Table II). With a surface tension value of 15 cal/mol Å^2 our predicted location of melittin agrees best with the adjusted experimental value of 18.2 Å. We also computed the difference between the solvation energies with our implicit membrane model and with an implicit homogeneous dielectric environment ($\varepsilon=80$) for the conformations sampled at the end of implicit membrane simulations of melittin (Table II). The free energy of partitioning of unfolded melittin in aqueous solvent into folded melittin in the membrane bilayer was estimated experimentally to be −7 to −8 kcal/mol.[67] With $\gamma=15$ cal/mol Å^2 we find a difference in solvation energy of −10 kcal/mol for the folded conformation between aqueous solvent and the membrane. In comparison to the experimental result this value is expected to overestimate the transfer free energy since we ignore the (positive) free energy contribution from folding melittin into its membrane-bound conformation in aqueous solvent in the absence of the membrane. While we cannot

TABLE II. Membrane position and transfer energy of melittin for different values of the empirical surface tension parameter γ. The positions $\bar{Z}_{MLT}$ of the geometric center of melittin are averaged over the last 2 ns of simulations. The transfer energy ΔE is computed as the difference between the solvation energy with the implicit membrane environment (E_m) and an implicit homogeneous aqueous environment ($\varepsilon=80, E_w$) for the melittin conformations sampled during the last 2 ns of implicit membrane simulations.

γ (cal/mol Å^2)	$\bar{Z}_{MLT}$ (Å)	$\Delta E = E_m - E_w$ (kcal/mol)
5	22.9	−1.34
10	20.5	−5.15
15	19.1	−10.1
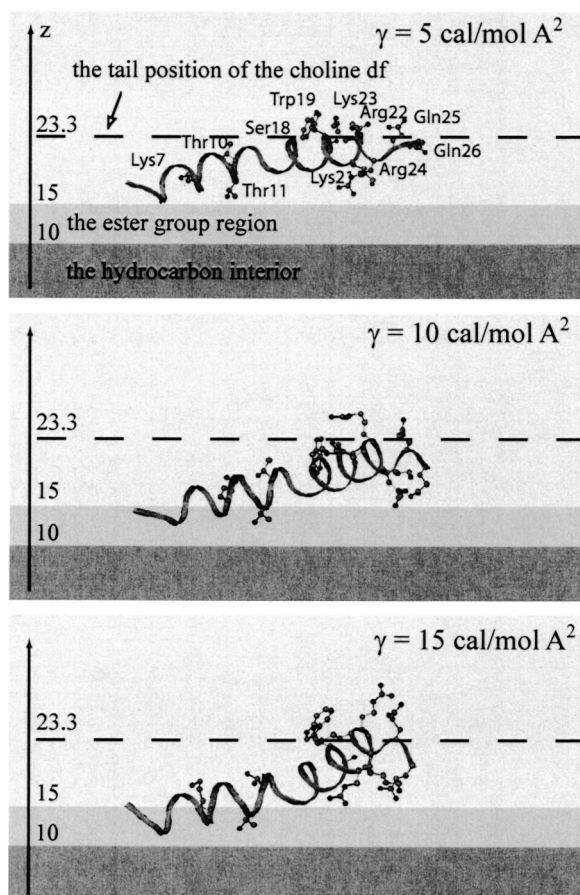
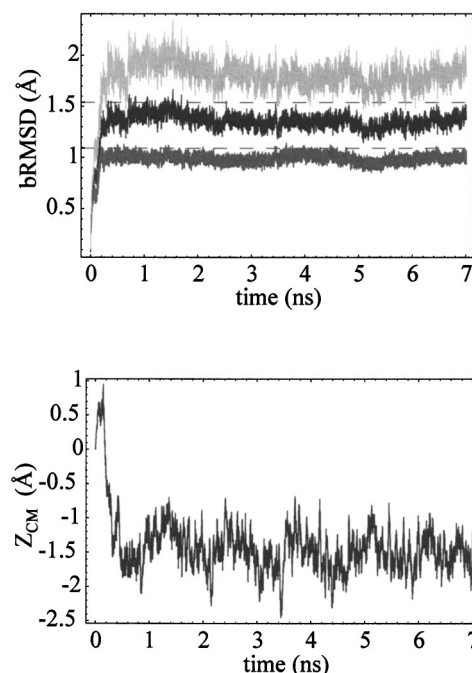FIG. 13. Snapshots of melittin at the end of 10 ns MD simulations.

FIG. 14. The backbone RMSD (top) and the z component of the center of mass (bottom) of bacteriorhodopsin from MD simulations. The surface tension parameter was set to 15 cal/mol Å^2. The bRMSD for all residues, TM residues, and non-TM residues are shown in black, dark gray, and light gray respectively. The dashed lines indicate the range of bRMSD from the explicit MD simulations of bacteriorhodopsin trimer (Ref. 69).

estimate the total transfer free energy of melittin from aqueous phase to membrane interface from the current study, our estimate for the transfer energy of the folded conformation of melittin appears to be in good qualitative agreement with the experimental data.

Figure 13 shows the snapshots of melittin at the end of 10 ns MD simulation in order to illustrate its relative orientation in the membrane. Previous 3.5 ns simulations of melittin with the two-dielectric implicit membrane model GBSW found the positions of the center of the mass of melittin to be in the region between 12.4 Å and 13.4 Å which is just above their membrane interface (12.5 Å) as well as 15.3 Å for a small kink angle conformation and 5.8 Å for a perpendicularly oriented conformation.[24] Their results agree with the 600 ps explicit MD simulation,[8] but not with the experimentally observed distributions of melittin in lipid bilayers.[66] The surface tension coefficient used in GBSW calculations[24] was rather high at 40 cal/mol Å^2, while we used values in the range from 5 to 15 cal/mol Å^2, In our model the use of a higher surface tension value would also drive the melittin position much closer to the membrane center (data not shown), but the choice of a high surface tension value would lead to larger deviations for the amino acid side chain test systems described above.

As mentioned above, we also performed a simulation of melittin with a corrected nonpolar contribution as shown in Fig. 10. In this case, the trajectory of the z component of geometrical center over 4 ns of MD simulation is located on

average ~ 1 Å closer to the membrane center for all three surface tension parameters $\gamma = 5$, $\gamma = 10$, and $\gamma = 15$ cal/mol Å^2. A shift closer to the membrane center with the altered profile is not surprising, since the nonpolar contribution is reduced in the region from $z = 5$ to $z = 15$ Å. With such a shift, the melittin center of mass is still very close to the experimental data, but it begins to approach the results from the explicit solvent simulations.

D. Molecular dynamics simulations of bacteriorhodopsin

One of the motivations for using the implicit solvent model over an explicit solvent representation is the possibility to perform molecular dynamics simulations of membrane-bound proteins or peptides that are not feasible with an explicit solvent simulation due to the size of the molecules and/or the length of the desired simulation time. In order to demonstrate that our model is applicable to the study of larger integral-membrane-bound proteins we have tested our new formalism on bacteriorhodopsin where extensive reference data is available from simulations with explicit water and lipids.[51,68,69]

Figure 14 shows the backbone root mean square deviation (bRMSD) and the z component of the center of mass over 7 ns of molecular dynamics simulation of bacteriorhodopsin with our implicit membrane HDGB model. We defined the transmembrane (TM) residues as residues whose C_α atoms were at the beginning of the simulation ($t = 0$) within the low-dielectric continuums, that is, the inner two slabs in Fig. 2(b) (the thickness of 30 Å.) The HDGB simulation of bacteriorhodopsin that was started from the experi-

mental structure remained stable throughout the simulation. The bRMSD of the mean structure computed from 2 to 7 ns was found to be 1.26 Å (0.92 Å for the transmembrane residues and 1.68 Å for non-TM residues). The average z component of the center of the mass was −1.51 Å. The total bRMSD of the mean structure from our simulation is comparable to the range of mean-structure bRMSD from 1.09 Å to 1.54 Å of the 5 ns explicit MD simulation of bacteriorhodopsin trimer,[69] while a 200 ps MD simulation with the empirical solvent-exclusion model of Lazaridis gave a total bRMSD of 2.96 Å. We note that the retinal was not included in the simulation performed by Lazaridis, which may explain the larger deviation from the experimental structure. These results suggest that our new formalism is well suited for the study of integral-membrane proteins.

V. DISCUSSIONS

The excellent agreement between our HDGB model and PB theory (Fig. 7) demonstrates that the idea of using an apparent dielectric constant profile may be used successfully for assigning a local dielectric constant to each solute atom in a heterogeneous dielectric environment and for computing effective atomic Born radii according to Eq. (6). This scheme effectively implements for the first time a heterogeneous dielectric environment within the generalized Born formalism, leading to a more realistic yet efficient model of biological membranes. The dielectric constant profiles used here are based on the three-dielectric model of the membrane-water environment. Our partitioning of biological membrane is based on dielectric profile data obtained by explicit molecular dynamics simulations.[22] We would like to point out, however, that there are many other possible ways of partitioning the membrane-water system into layers of dielectric slabs. An arbitrary modification to a different partitioning scheme of the membrane-water system (both in terms of dielectric constants and widths of continuum slabs) is straightforward, and not limited in any way by the new scheme proposed here. This leaves the exact choice of the dielectric profile as a tunable feature of an implicit membrane model, which can be adjusted to match experimental data in future studies. We note that a two-dielectric model of biological membranes, as used in previous efforts, appears to be a poor approximation (see Fig. 3). Existing schemes[24,25,27] are also limited by the fact that they require that the membrane and the solute cavity have the same dielectric constant in order to arrive at a two-dielectric representation.

Although our membrane GB model provides a flexible scheme of describing biological membranes, the model still lacks some important features such as the surface charge distribution of the head group region and dynamic modulations of membrane surfaces, which are found *in vivo*. The effect of the surface charge distribution, for example, is important in aggregation of β-amyloid peptides on membrane surface.[70] However, in principle, it is possible to include such effects with an implicit inclusion of salt effects based on Debye–Hückel theory.[71] We also point out that our implicit membrane GB model cannot be applied directly to transmembrane proteins with channels such alamethicin[72] or

KcsA channel.[73] In these cases, explicit solvent molecules would have to be added in the channel region, which is feasible, but introduces additional technical challenges.

Many issues remain to be addressed in future developments of our new implicit membrane model. As mentioned above, the change of the effectively excluded molecular volume upon membrane insertion needs to be investigated in more detail. Another important issue is the choice of appropriate values for the friction coefficients used in Langevin molecular dynamics. In this study, we assumed the same friction coefficients inside and outside of membranes. Recently, the separation of the nonpolar interaction term into two distinct terms, a solute-solvent van der Waals term and a cavity formation term, was shown to be important in modeling energetics of proteins.[16,28] This may contribute significantly to results of simulations of transmembrane proteins and we are planning to test these ideas in the context of our membrane model as well.

Overall, our new implicit model for biological membranes appears to capture the salient features of such systems. The development of implicit models for membranes is motivated by the possibility to perform MD simulations of large-size transmembrane proteins that are not feasible by conventional explicit MD simulations. We have demonstrated the applicability of our implicit membrane HDGB model to the simulation of membrane-bound peptides and integral membrane proteins by showing the stability of molecular dynamics simulations of melittin and bacteriorhodopsin.

VI. CONCLUSION

We propose a modification of the standard GB theory that can be applied to the heterogeneous dielectric environment generated by lipid membrane and water. The membrane-water system was described as a layer of dielectric continua of three distinct dielectric constants (hydrocarbon interior, ester group region, and high dielectric region). The apparent dielectric constant profile was introduced for calculating the effective atomic Born radii in such a multidielectric environment. The proposed modification was successful in predicting the electrostatic contribution of solvation free energy of the M2 channel-lining segment from nicotinic acetylcholine receptors with a relative error of 0.17% compared to the exact finite-difference solution of the Poisson equation. Langevin molecular dynamics simulations of melittin and bacteriorhodopsin were stable over the entire simulation time of 10 ns and 7 ns, respectively. In melittin simulations the location of center of melittin along the membrane normal remained in excellent agreement with the experimentally determined distribution, especially when an empirical surface tension parameter of 15 cal/mol Å^2 was used. The solvation free energy profile of a water molecule, however, shows that care must be taken to apply our model to a small molecule such as water since the effect of the molecular volume change from bulk water region to lipid membrane on the transfer solvation energy may not be negligible. When the effect of volume change was taken care appropriately, the transfer free energy of the amino acid side chain analogs

predicted by our model qualitatively agrees with the experimental result of the transfer free energy from cyclohexane to water. We plan to investigate the extent of the change in excluded molecular volume between water and membrane phases to address this issue in a future study.

ACKNOWLEDGMENTS

[1] A. Leach, *Molecular Modelling: Principles and Applications*, 2nd ed. (Pearson Education, Harlow, England, 2001); A. Warshel, Acc. Chem. Res. **35**, 385 (2002).

[2] T. Hansson, C. Oostenbrink, and W. F. van Gunsteren, Curr. Opin. Struct. Biol. **12**, 190 (2002).

[3] L. R. Forrest and M. S. P. Sansom, Curr. Opin. Struct. Biol. **10**, 174 (2000).

[4] C. L. Brooks and M. Karplus, J. Mol. Biol. **208**, 159 (1989).

[5] B. L. de Groot and H. Grubmuller, Science **294**, 2353 (2001).

[6] S. Berneche and B. Roux, Nature (London) **414**, 73 (2001).

[7] B. Roux and T. Simonson, Biophys. Chem. **78**, 1 (1999); M. Schaefer and M. Karplus, Biophys. Chem. **100**, 1578 (1996).

[8] S. Berneche, M. Nina, and B. Roux, Biophys. J. **75**, 1603 (1998).

[9] W. Rocchia, E. Alexov, and B. Honig, J. Phys. Chem. B **105**, 6507 (2001); M. K. Gilson and B. Honig, Proteins: Struct., Funct., Genet. **4**, 7 (1988); M. E. Davis and J. A. McCammon, J. Comput. Chem. **10**, 386 (1989).

[10] M. Feig, A. Onufriev, M. S. Lee *et al.*, J. Comput. Chem. **25**, 265 (2004).

[11] F. Fogolari, A. Brigo, and H. Molinari, Biophys. J. **85**, 159 (2003).

[12] B. Z. Lu, W. Z. Chen, C. X. Wang *et al.*, Proteins: Struct., Funct., Genet. **48**, 497 (2002); R. Luo, L. David, and M. K. Gilson, J. Comput. Chem. **23**, 1244 (2002).

[13] I. Oren, S. J. Fleishman, A. Kessel *et al.*, Biophys. J. **87**, 768 (2004).

[14] W. C. Still, A. Tempczyk, R. C. Hawley *et al.*, J. Am. Chem. Soc. **112**, 6127 (1990).

[15] M. S. Lee, M. Feig, F. R. Salsbury *et al.*, J. Comput. Chem. **24**, 1348 (2003).

[16] E. Gallicchio and R. M. Levy, J. Comput. Chem. **25**, 479 (2004).

[17] A. Onufriev, D. Bashford, and D. A. Case, J. Phys. Chem. B **104**, 3712 (2000).

[18] M. Feig, A. D. MacKerell, and C. L. Brooks, J. Phys. Chem. B **107**, 2831 (2003).

[19] A. Onufriev, D. A. Case, and D. Bashford, J. Mol. Biol. **325**, 555 (2003); J. A. Zhu, Y. Y. Shi, and H. Y. Liu, J. Phys. Chem. B **106**, 4844 (2002); B. N. Dominy and C. L. Brooks, *ibid.* **103**, 3765 (1999); N. Calimet, M. Schaefer, and T. Simonson, Proteins: Struct., Funct., Genet. **45**, 144 (2001); M. Y. Shen and K. F. Freed, Biophys. J. **82**, 1791 (2002).

[20] M. Feig and C. L. Brooks, Proteins: Struct., Funct., Genet. **49**, 232 (2002); L. R. Forrest and T. B. Woolf, *ibid.* **52**, 492 (2003); J. Zhu, Q. Q. Zhu, Y. Y. Shi *et al.*, *ibid.* **52**, 598 (2003); A. V. Morozov, T. Kortemme, and D. Baker, J. Phys. Chem. B **107**, 2075 (2003); A. K. Felts, E. Gallicchio, A. Wallqvist *et al.*, Proteins: Struct., Funct., Genet. **48**, 404 (2002); A. Fiser, M. Feig, C. L. Brooks *et al.*, Acc. Chem. Res. **35**, 413 (2002); B. N. Dominy and C. L. Brooks, J. Comput. Chem. **23**, 147 (2002).

[21] K. L. Mardis, R. Luo, and M. K. Gilson, J. Mol. Biol. **309**, 507 (2001); P. Ferrara, H. Gohlke, D. J. Price *et al.*, J. Med. Chem. **47**, 3032 (2004); S. Donnini and A. H. Juffer, J. Comput. Chem. **25**, 393 (2004); H. Gohlke and D. A. Case, *ibid.* **25**, 238 (2004); T. Lazaridis, Curr. Org. Chem. **6**, 1319 (2002).

[22] H. A. Stern and S. E. Feller, J. Chem. Phys. **118**, 3401 (2003).

[23] F. Zhou and K. Schulten, J. Phys. Chem. **99**, 2194 (1995).

[24] W. Im, M. Feig, and C. L. Brooks, Biophys. J. **85**, 2900 (2003).

[25] V. Z. Spassov L. Yan, and S. Szalma, J. Phys. Chem. B **106**, 8726 (2002).

[26] W. Im and C. L. Brooks, J. Mol. Biol. **337**, 513 (2004).

[27] T. Lazaridis, Proteins: Struct., Funct., Genet. **52**, 176 (2003).

[28] R. M. Levy, L. Y. Zhang, E. Gallicchio *et al.*, J. Am. Chem. Soc. **125**, 9523 (2003).

[29] P. A. Kollman, I. Massova, C. Reyes *et al.*, Acc. Chem. Res. **33**, 889 (2000).

[30] R. Constanciel and R. Contreras, Theor. Chim. Acta **65**, 1 (1984).

[31] D. Bashford and D. A. Case, Annu. Rev. Phys. Chem. **51**, 129 (2000).

[32] A. Onufriev, D. A. Case, and D. Bashford, J. Comput. Chem. **23**, 1297 (2002).

[33] T. Grycuk J. Chem. Phys. **119**, 4817 (2003).

[34] M. Feig and C. L. Brooks, Curr. Opin. Struct. Biol. **14**, 217 (2004).

[35] M. Feig, W. Im, and C. L. Brooks, J. Chem. Phys. **120**, 903 (2004).

[36] J. G. Kirkwood, J. Chem. Phys. **2**, 351 (1934).

[37] J. F. Nagle and S. Tristram-Nagle, Biochim. Biophys. Acta **1469**, 159 (2000).

[38] M. Born, Z. Phys. **1**, 45 (1920).

[39] R. L. Burden and J. Douglas Faires, *Numerical Analysis*, 5th ed. (PWS-Kent, Boston, 1993).

[40] D. Sitkoff, K. A. Sharp, and B. Honig, J. Phys. Chem. **98**, 1978 (1994).

[41] P. Ferrara, J. Apostolakis, and A. Caflisch, Proteins: Struct., Funct., Genet. **46**, 24 (2002).

[42] B. Roux, Biophys. J. **73**, 2980 (1997).

[43] S. J. Marrink and H. J. C. Berendsen, J. Phys. Chem. **100**, 16729 (1996).

[44] A. Bennaim and Y. Marcus, J. Chem. Phys. **81**, 2016 (1984).

[45] X. L. Cheng, V. Hornak, and C. Simmerling, J. Phys. Chem. B **108**, 426 (2004); J. W. Pitera and W. Swope, Proc. Natl. Acad. Sci. U.S.A. **100**, 7587 (2003); R. H. Zhou and B. J. Berne, *ibid.* **99**, 12777 (2002).

[46] B. R. Brooks, R. E. Bruccoleri, B. D. Olafson *et al.*, J. Comput. Chem. **4**, 187 (1983).

[47] A. D. MacKerell, D. Bashford, M. Bellott *et al.*, J. Phys. Chem. B **102**, 3586 (1998).

[48] F. M. Marassi, J. J. Gesell, A. P. Valente *et al.*, J. Biomol. NMR **14**, 141 (1999); S. J. Opella, F. M. Marassi, J. J. Gesell *et al.*, Nat. Struct. Biol. **6**, 374 (1999).

[49] W. Im, D. Beglov, and B. Roux, Comput. Phys. Commun. **111**, 59 (1998); M. Nina, D. Beglov, and B. Roux, J. Phys. Chem. B **101**, 5239 (1997).

[50] H. J. C. Berendsen, J. P. M. Postma, M. F. van Gunsteren *et al.*, presented at the The Jerusalem Symposium on Quantum Chemistry and Biochemistry, Jerusalem, Israel, 1981 (unpublished).

[51] J. Saam, E. Tajkhorshid, S. Hayashi *et al.*, Biophys. J. **83**, 3097 (2002).

[52] T. C. Terwilliger and D. Eisenberg, J. Biol. Chem. **257**, 6010 (1982); **257**, 6016 (1982).

[53] H. Belrhali, P. Nollert, A. Royant *et al.*, Structure (London) **7**, 909 (1999).

[54] K. Gerwert, B. Hess, J. Soppa *et al.*, Proc. Natl. Acad. Sci. U.S.A. **86**, 4943 (1989).

[55] J. P. Ryckaert, G. Ciccotti, and H. J. C. Berendsen, J. Comput. Phys. **23**, 327 (1977).

[56] S. J. Marrink and H. J. C. Berendsen, J. Phys. Chem. **98**, 4155 (1994).

[57] P. Hochtl, S. Boresch, W. Bitomsky *et al.*, J. Chem. Phys. **109**, 4927 (1998).

[58] G. Hummer, L. R. Pratt, and A. E. Garcia, J. Phys. Chem. **99**, 14188 (1995); S. W. Rick and B. J. Berne, J. Am. Chem. Soc. **116**, 3949 (1994).

[59] D. Bemporad, J. W. Essex, and C. Luttmann, J. Phys. Chem. B **108**, 4875 (2004).

[60] M. R. Shirts, J. W. Pitera, W. C. Swope *et al.*, J. Chem. Phys. **119**, 5740 (2003).

[61] G. V. Heijne, Annu. Rev. Biophys. Biomol. Struct. **23**, 167 (1994).

[62] C. Landoltmarticorena, K. A. Williams, C. M. Deber *et al.*, J. Mol. Biol. **229**, 602 (1993).

[63] S. H. White and R. E. Jacobs, Biophys. J. **53**, A631 (1988); W. M. Yau, W. C. Wimley, K. Gawrisch *et al.*, Biochemistry **37**, 14713 (1998).

[64] A. Grossfield and T. B. Woolf, Langmuir **18**, 198 (2002).

[65] W. C. Wimley and S. H. White, Biochemistry **31**, 12813 (1992); **32**, 6307 (1993); Nat. Struct. Biol. **3**, 842 (1996); W. C. Wimley, T. P. Creamer, and S. H. White, Biochemistry **35**, 5109 (1996).

[66] K. Hristova, C. E. Dempsey, and S. H. White, Biophys. J. **80**, 801 (2001).

[67] A. S. Ladokhin and S. H. White, J. Mol. Biol. **285**, 1363 (1999).

[68] J. Baudry, E. Tajkhorshid, F. Molnar *et al.*, J. Phys. Chem. B **105**, 905 (2001); H. Jang, P. S. Crozier, M. J. Stevens *et al.*, Biophys. J. **87**, 129 (2004).

[69] C. Kandt, J. Schlitter, and K. Gerwert, Biophys. J. **86**, 705 (2004).

[70] M. Bokvist, F. Lindstrom, A. Watts *et al.*, J. Mol. Biol. **335**, 1039 (2004).

[71] J. Srinivasan, M. W. Trevathan, P. Beroza *et al.*, Theor. Chem. Acc. **101**, 426 (1999).

[72] A. Kessel, D. P. Tieleman, and N. Ben-Tal, Eur. Biophys. J. **33**, 16 (2004).

[73] B. Roux, Curr. Opin. Struct. Biol. **12**, 182 (2002).

[74] A. Radzicka and R. Wolfenden, Biochemistry **27**, 1664 (1988).